The effect of Si incorporation on the mechanical properties and corrosion behaviour of a-C:H and a-C:H:Si coatings

L. COSTINESCU[a], C. COJOCARIU[a], M. DUDITA[b], L. PARV[c], I. L. VELICU[d], D. MUNTEANU[a*]
[a]*Department of Materials Science, Transilvania University, 500036 Brasov, Romania*
[b]*Department of Renewable Energy Systems and Recycling, Transilvania University, 500036 Brasov, Romania*
[c]*Department of Manufacturing Engineering, Transilvania University, 500036 Brasov, Romania*
[d]*Department of Physics, Alexandru Ioan Cuza University, 700506 Iasi, Romania*

This paper aims to present the corrosion behaviour and mechanical properties of hydrogenated amorphous carbon films (a-C:H) and Si incorporated hydrogenated amorphous carbon (a-C:H:Si) coatings. The a-C:H and a-C:H:Si top coatings were deposited on 100Cr6 steel substrates (using also interlayers) by plasma assisted chemical vapour deposition technique. In terms of mechanical properties, nanoindentation hardness, elastic modulus and adherence were measured. The corrosion behaviour was evaluated using both salt spray test method and electrochemical corrosion test (potentiostatic method). According to the experimental results, the addition of Si into a-C:H films improves the corrosion resistance of these ones in comparison with the variants without Si. However, the addition of Si produces a light decrease of the mechanical properties.

(Received November 14, 2014; accepted January 21, 2015)

Keywords: Corrosion resistance, Hardness, Hydrogenated amorphous carbon, Young's modulus

1. Introduction

Carbon based, e.g., diamond-like carbon coatings (DLC, a-C:H, a-C) are entering into broad fields of applications due to the combination of valuable properties, such as high hardness and elasticity, wear resistance and chemical inertness. This is why diamond-like carbon coatings have been the subject of intense research over the last two decades [1–4]. The incorporation of specific additional elements into DLC films can advantageously modify the properties of this widely studied group of materials [1–6]. Si-containing amorphous hydrogenated carbon films are known to have high wear resistance [7, 8], reduced friction (even in humid air) [3, 9], reduced surface tension [10, 11] and low residual internal stress [12–15].

The introduction of Si into a-C:H films can lead to a significant improvement of the corrosion resistance of the films by increasing the charge transfer resistance and decreasing anodic current in polarization. This could be attributed to the formation of a denser coating, thus impeding the penetration of water molecules or ions as Si addition has a beneficial effect on promoting surface nucleation which diminishes the production of pores, therefore improving surface roughness [16-18].

This paper is focused on the innovative multifunctional based on the a-C:H:Si system coatings' efficiency to protect surfaces against fretting and corrosion degradation.

2. Experimental details

Three sets of DIN-100Cr6 bearing steel samples (5 for each set) were prepared for deposition of a-C:H (the first set) and a-C:H:Si (the second set) tribological coatings. The third set of samples was kept uncoated, as a reference sample set. All the depositions (sets 1 and 2) were carried out in industrial PVD/PACVD equipment from the Oerlikon-Balzers group. Before the deposition, all the samples have been hardened and low tempered, obtaining a hardness of 63 HRC and an average roughness Ra=0.06μm on the substrate surface for deposition.

For all the samples, a thin-adherence layer (CrC) is deposited previously by PVD-sputtering (standard Cr target with arc-pulsed bias AC-100V). Plasma assisted chemical vapour deposition (PACVD) is used to build up the effective tribological carbon coating on top. In contrast to conventional combination coatings, these multifunctional coatings are the result of a single process that yields homogeneous, defect-free coatings of uniquely high quality and adhesion strength. The PVD - PACVD transition process occurs at a mean voltage of -500V. For the adhesion layer deposition, Cr-targets run parallel with a reactive C_2H_2 gas flow (standard gas flow 450 sccm). An a-C:H topcoat was deposited by PACVD using acetylene (C_2H_2) as precursor gas. The a-C:H growth starts at medium gas flow (around 200 sccm). The depositions were carried out for one hour at a constant pressure of 1Pa, keeping the temperature constant at 180^{o}C. The argon flow was fixed at 60 sccm and the acetylene flow was kept constant at 5 sccm.

For one of the two sets of samples (a-C:H:Si variant), an intermediate layer – Si-C:H type, has been deposited after CrC to accommodate in better conditions Si-DLC, using a gas atmosphere based on tethrametylsilane (TMS) – $Si(CH_3)_4$. Finally, the Si-DLC top film has been prepared with gaseous mixture athmosphere of TMS and acetylene (C_2H_2).

The film's thickness was measured using the CALOTEST method (CSM Instruments).

The surface chemical composition of the as-deposited samples was investigated by X-ray photoelectron spectroscopy (XPS). The XPS analysis was performed by an Escalab MkII system. The spectra were acquired using an Al anode (Kα radiation line at 1486.6eV unmonochromatised) as X-ray source operating at a voltage of 14.5 kV and a power of 230 W.

The thin films' surface morphology, roughness and microstructural properties were investigated through atomic force microscopy - AFM (NT–MDT NTGRA PRIMA EC system) and completed by scanning electron microscopy – SEM analysis. The AFM system was operated in semicontact mode, for a scanning rate of 1 Hz and it was also used to characterize the uniformity and grain size of a-C:H and a-C:H:Si thin films. Multiple scans were performed for different 5 µm x 5 µm contact areas. In order to evaluate the pore size distribution, the image analysis was carried using a WSxM software.

The corrosion behaviour was evaluated using two methods: salt spray test (SST) and electrochemical corrosion test (potentiostatic method). The SST was performed according to DIN EN ISO 9227 using a Vötsch VSC 450 Salt Spray Chamber. The equipment used for the potentiostatic test is a multichannel potentiostat galvanostat (PAR BioLogic VSP) equipped with a standard three-electrode electrochemical cell: a working electrode (sample), a counter electrode (white platinum, S=1 cm^2) and a reference electrode (saturated standard calomel electrode-SCE, ESCE = 0.244 V vs. NHE). The working electrode was polarized from cathodic to anodic potential (-1… +1 V) with a scan rate of 50 mV/s. The Tafel plots were used to determine the corrosion potential (E_{corr}) and current (I_{corr}). Thus, the values of the thermodynamic and kinetic parameters (E_{corr} and the density of the corrosion current, j_{corr}) were determined by interpolation from the Tafel polarization curves. The relation used to calculate the density of the corrosion current (for a sample with surface area -A) is:

$$j_{corr} = \frac{I_{corr}}{A_{sample}} \quad (1)$$

All corrosion experiments were carried out at room temperature, in 5% NaCl aqueous solution, the standard concentration for simulating an aggressive saline environment [19].

The nanoindentation tests (for establishing the films indentation hardness H and the reduced elastic modulus E_r) and micro-scratch measurements (for establishing the adherence) have been carried out using a CSM instruments Compact platform containing a Nanoidenter - NHT2 with application loads from 1 mN to 500 mN) and a Micro-Scratch Rockwell head (MST with application loads from 0.03 N to 30 N. The nanoindentation system constantly records the penetration depth of the indenter as a function of the applied load. In order to avoid the residual viscoelasticity, the loading and unloading processes were separated by 5 seconds holding time. The H and E_r were determined from the loading and unloading curves, based on the Oliver-Pharr method [20-26]. According to these, the reduced modulus, E_r, is given by:

$$E_r = \frac{\sqrt{\pi}}{2} \cdot \frac{S}{\sqrt{A_c}} = \frac{\sqrt{\pi}}{2} \cdot \frac{1}{C} \cdot \frac{1}{\sqrt{A_c}} \quad (2)$$

which can be calculated having derived S and A_C from the indentation curve using the area function, A_C being the projected contact area.

The coating (material) Young's modulus, E, can then be obtained then from:

$$\frac{1}{E_r} = \frac{1-\nu^2}{E} + \frac{1-\nu_i^2}{E_i} \quad (3)$$

where E_i and ν_i are the Young's modulus and Poisson coefficient of the indenter and ν the Poisson coefficient of the tested sample.

The adhesion/cohesion of the films was evaluated through the scratch-test technique, using the Revetest method (CSM Instruments) [27]. The load was increased linearly from 0 to 30 N (Rockwell C 200 mm radius indenter tip, loading speed of 10 N/min and scratch speed of 1 mm/min). In this case, the minimum load L_c (critical load) at which on the film appeared the first delamination has been taken into consideration and represents the film-substrate adhesion strength. In fact, the critical loads L_c values corresponding to the adhesive failure mechanisms were measured by analysing the failures events in the scratch track by optical microscopy. In what the critical loads L_c, are concerned, generally, there are three parameters L_{c1}, L_{c2} and L_{c3}, which are taken into account, and represent the load corresponding to apparition of the first cracking (L_{c1}), the load for first delamination (L_{c2}) and the load for full delamination (L_{c3}) [27]. In the present work, L_c represents actually the L_{c2} critical load.

3. Results and discussion

3.1 Compositional and structural features

Table 1 presents a summary of the prepared samples with resulting compositions.

Table 1.The as-deposited coating's composition and thickness

Coating type	*Composition (at.%)*				*Average thickness (µm)*
	Si	C	O	Cr	
a-C:H:Si	3.6	76.2	17.16	3.04	4.06
a-C:H	-	79.59	17.19	3.22	2.12

Figs. 1(a) and 1(b) present the bonding ratio (sp^3/sp^2) with an average value of 0.97 for a-C:H coatings (Si = 0 at. %) and 1.84 for a-C:H:Si coating (Si= 3.6 at.%). As can be seen, the bonding ratio (sp^3/sp^2) of a-C:H:Si thin films increases with the Si incorporation. This last conclusion has been related also by other researches, such as Ho-Gun Kim et al. [27].

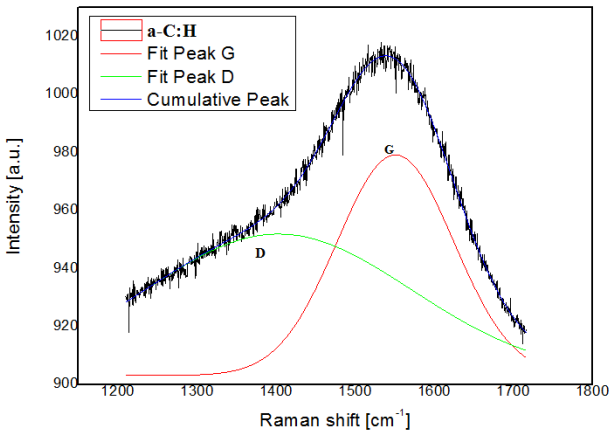

(a)

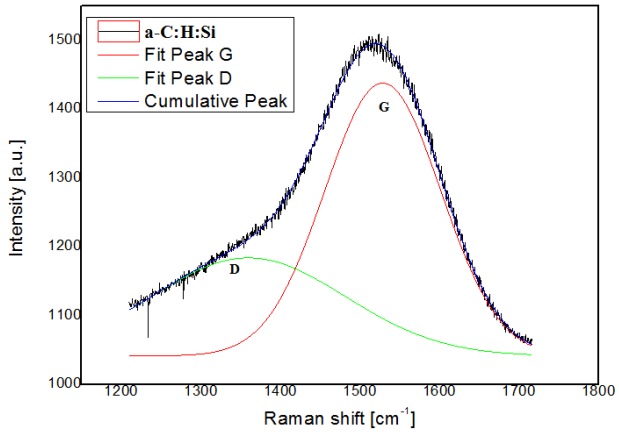

(b)

Fig. 1. The Raman experimental spectra resulted for both categories of coatings: a-C:H (a) and a-C:H:Si thin films (b).

According to the literature, a typical a-C:H coating Raman spectrum is composed of two bands: one for <graphite>centered at ~1580 cm^{-1} (G-band) and one for <disorder>centered at ~1350 cm^{-1} (D-band) [29]. Taking into account the obtained results, the Raman spectra of the a-C:H films indicate the presence of the sp^2 carbon embedded in sp^3 bonded matrix. The fraction of sp^3 bonding contained in the film can be evaluated by the 'G' peaks position. By correlating the Full Width at Half Maximum (FWHM) and the relative intensity of 'D' and 'G' peaks, the formation of sp^3 bonds can be evaluated [30]. In order to extract the exact position of the two bands, the results were fitted with two Gaussian functions. The presence of a very large band centred at ~1560 cm^{-1} which is not symmetric was observed in the case of both samples and is in concordance with the amorphous structure of the films [31]. The contribution of another band ~1350 cm^{-1} (corresponding to the D band) can explain the asymmetry of the band at 1560 cm^{-1}.

Table 2 shows the average sp^3 bonds content of each type of coating. The highest content of sp^3 bonds was obtained for the a-C:H:Si variant. This is directly related to the deposition conditions. A higher concentration of C_2H_2 in the gas mixture may lead to more sp^3 bonds of the diamond type.

Table 2. The Raman spectra parameters and average results of the film's sp^3 bonds content

Coating	*a-C:H*	*a-C:H:Si*
I(G) [cm^{-1}]	1550.8	1528.7
FWHM_G [cm^{-1}]	171.3	171.6
I (D) [cm^{-1}]	1394.8	1359.8
FWHM_D [cm^{-1}]	403.6	286.8
sp^3 content [%]	0.97	1.84

3.2 Topography and porosity

It is commonly accepted that the thin films surface morphology has a marked influence on the corrosion activity.

For a high corrosion resistance, the films have to be very compact (should have a very small porous nano-/meso-/microstructure).

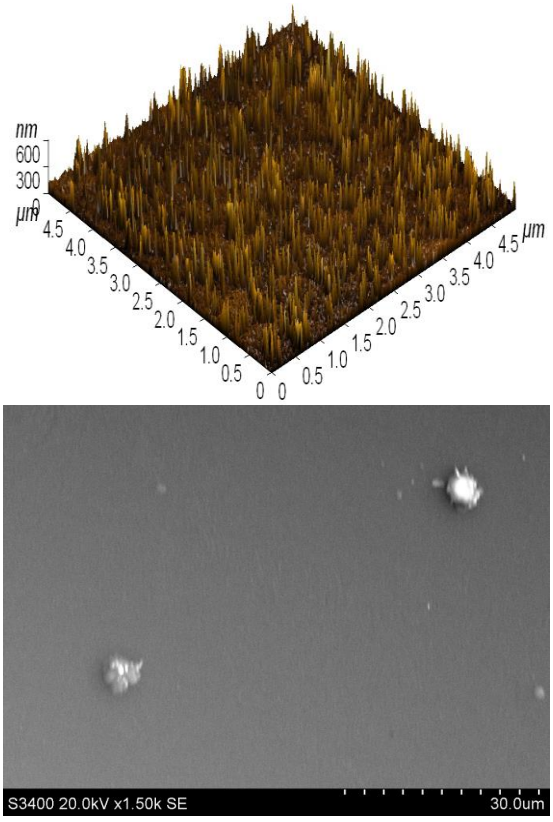

Fig. 2. AFM and SEM images for a-C:H sample.

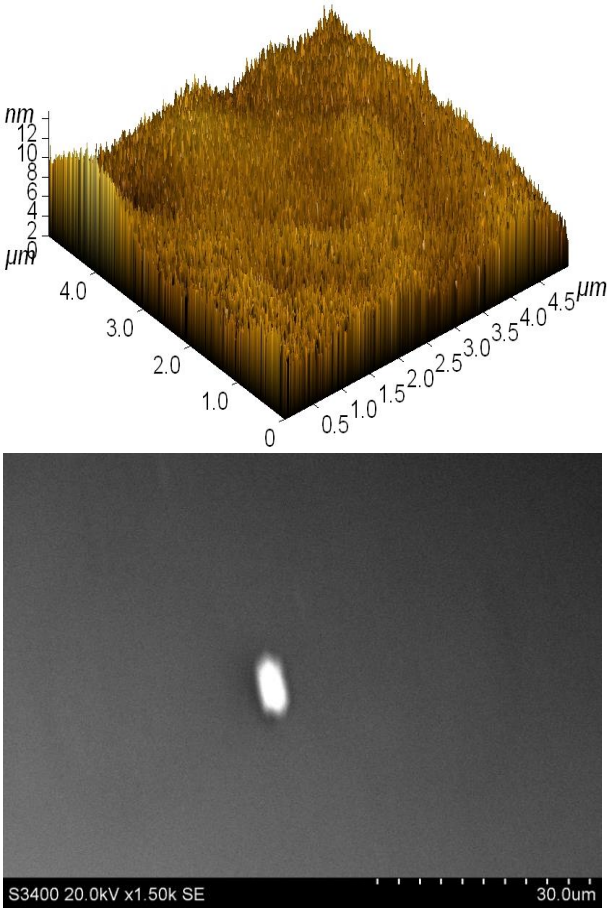

Fig. 3. AFM and SEM images for a-C:H:Si sample.

Figs. 2 and 3 present the representative SEM and 3D-AFM images for a-C:H and a-C:H:Si obtained coatings. For both variants, the results revealed that, in generally, the films are uniformly distributed on the substrate-surface. Small defects have been detected from place to place, with a higher tendency for a:C:H films. In fact, the much compacted aspect of a-C:H:Si thin-films is sustained also by the lower roughness values registered by AFM in this case. The surface morphology of Si-DLC coatings indicates a smaller pitting area and evidence of less amount penetration of water and ions as shown in figure 3.

The columnar structure obtained after deposition it can be clearly noticed for both samples. The figure 4 presents the average results for pore size analysis, for a-C:H (a) and a-C:H:Si (b) coatings. According to these results, the nanoporosity is far from being clearly and sharply defined. The film's narrow pore size distribution presents a high importance for its catalytic activity implying good homogeneity in the pore structure, mainly for a-C:H:Si. The pore size distribution is much broader for a-C:H sample, indicating a more irregular and less ordered structure; this aspect is confirmed also by the structure obtained by Raman procedure (more amount of sp^2 clusters). The surface becomes smoother, and defects vanish with increasing Si content (regular structure - more sp^3 clusters).

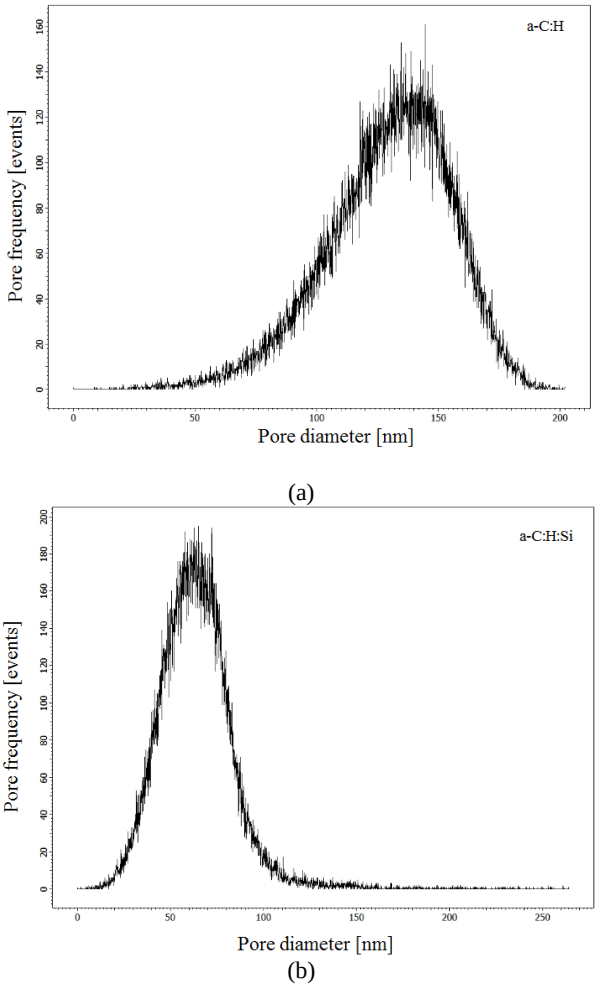

Fig.4. Pore size distribution obtained by AFM analysis for a-C:H (a) and a-C:H:Si (b) coatings.

3.3 Corrosion behaviour

The coating topography, degree of compaction and chemical composition strongly influence its properties, especially the corrosion behaviour in aggressive environments [32]. The corrosion tests performed according to the experimental details demonstrate that the best corrosion behaviour have been obtained for the a-C:H:Si coatings.

In this respect, Table 3 reveals the corrosion parameters for the investigated surfaces.

Table 3.Corrosion parameters obtained by electrochemical method

Coating	Corrosion parameters			
	E_{corr} [mV]	j_{corr} [mA/m^2]	β_c [mV]	β_a [mV]
uncoated	-876	525	63	879
a-C:H	-403	4	166	161
a-C:H:Si	-371	0.3	204	106

By comparing the obtained values with the standard electrode potentials, the surface oxidation reactions involved at the metal /corrosive agent interface can be discussed. Besides iron, the possible participation of the co-metals presented in the alloy or as component in the surface coating must be considered. If a protective coating is deposited on the substrate, an anodic shift of the corrosion potential is observed. This corresponds to a reduction of the thermodynamic activity of the metallic surface and results in a significant reduction of the corrosion rate. The modification of E_{corr} is given by the presence of the elements with high corrosion resistance such as chromium or tungsten, but also by the carbon sp^3 species which can complicate the corrosion mechanism. This mechanism involves chemical reactions that take place with different reaction rates, depending on the coating's properties – film's composition and thickness, and porosity.

Fig. 5 presents the Tafel curves for uncoated, only a-C:H and a-C:H:Si samples.

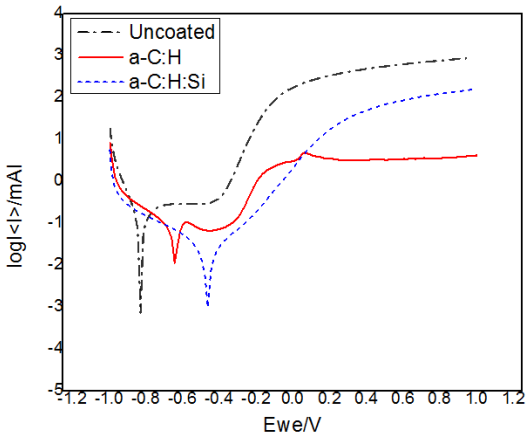

Fig.5. Tafel curves for uncoated, a-C:H and a-C:H:Si coatings.

All the coated samples present better corrosion behaviors in comparison with the uncoated steel. The differences in the Tafel slopes for the anodic, respectively cathodic processes are in accordance with the corrosion rate: higher for the sample a-C:H comparing to a-C:H:Si. This suggests a more rapidly dissolution mechanism of the metallic surface for a-C:H. Most likely the deposition processes lead to porous surfaces and defects such as pinholes and damage zones with lower corrosion resistance, confirmed also by the porosity distribution analysis. On the other hand increasing Si content led to an increase in the dense sp^3 bonding and a decrease in the percentage and dimensions of those defects. Xu et al. [33] have also shown that the result is corresponded to the report, which higher bonding ratio (sp^3/sp^2) enhanced the corrosion resistance.

The average mass loss of the films is about 19.25 g/m^2 for the a-C:H samples and 15.82 g/m^2 for the a-C:H:Si samples, respectively (area exposed 0.001875 m^2). Correlating the salt spray test results with the electrochemical test results, the sample with the best corrosion resistance is the a-C:H:Si. The presence of Si improves the resistance of this sample to corrosion in saline environments.

3.4 Hardness and elastic modulus

Figs. 6(a) and 6(b) present the dependences of hardness and reduced elastic modulus on the normalized depth *h/t* (where h is the depth position of the indenter penetration and t the coating thickness). For very small indentation depths, H and E_r values increase with the increasing of indentation depth, reaching their maximum values (H = 25 GPa, E_r= 193 GPa for a-C:H sample and H= 18 GPa, E_r= 159 GPa for a-C:H:Si sample) in the region of top DLC coating. This tendency of increasing for H and $E_r$in this superficial region may be attributed to the surface roughness and imperfections. The H and E_r values remain approximately constant along of top-coating thickness, for both categories of coatings.

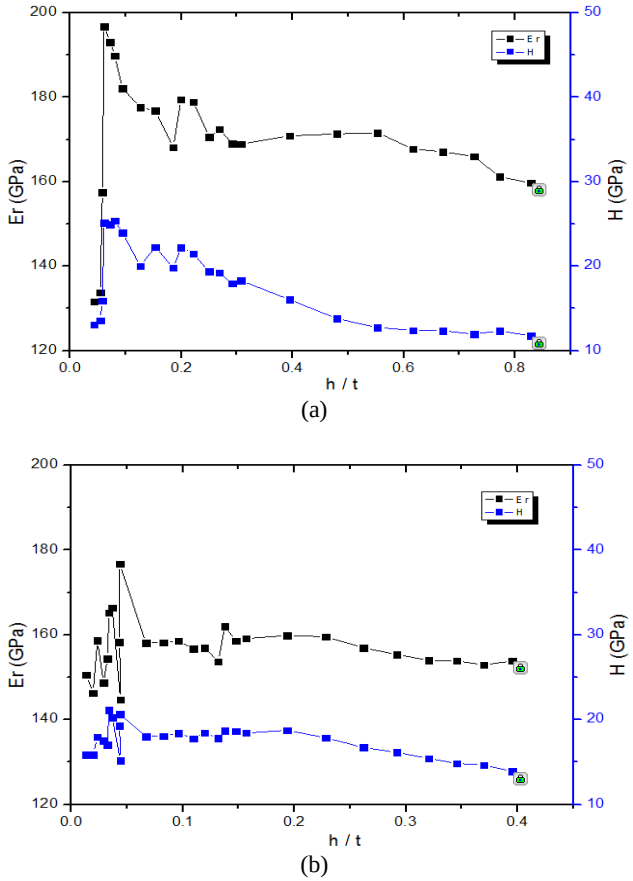

Fig.6. The variation of hardness and elastic modulus with the normalized depth for (a) a-C:H and (b) a-C:H:Si coatings.

For both cases, the hardness and reduced elastic modulus values decrease in depth, once it is reached the complementary films (intermediary and adhesion films) of each system. At maximum, the hardness is slowly higher for a-C:H coatings in comparison with a-C:H:Si variants, even the last ones are more compacted. This could be explained taking into account the possible influence of the

intermediary layer Si-C:H type. The same remarks are valid for the reduced elastic modulus.

Considering the registered reduced elastic modulus values, the average effective Young's modulus values – E could be estimated, based on equation 3. It is about 211 GPa for the a-C:H coatings and 162 GPa for a-C:H:Si.

3.5 Adhesion

The figures 7(a) and 7(b) present the failures associated to the L_c values, for the two kinds of coatings, (a-C:H and a-C:H:Si) along the scratch track; according to the registered results, the first delamination of the a-C:H coating was registered for an applied load of 10 N and, of 8 N for the a-C:H:Si coatings respectively. We could conclude here that the presence of Si in the coating composition leads to a light decreasing of its adhesion. Taking into account all the results, there is a tendency for mechanical properties comedown by adding silicon in these DLC coating types.

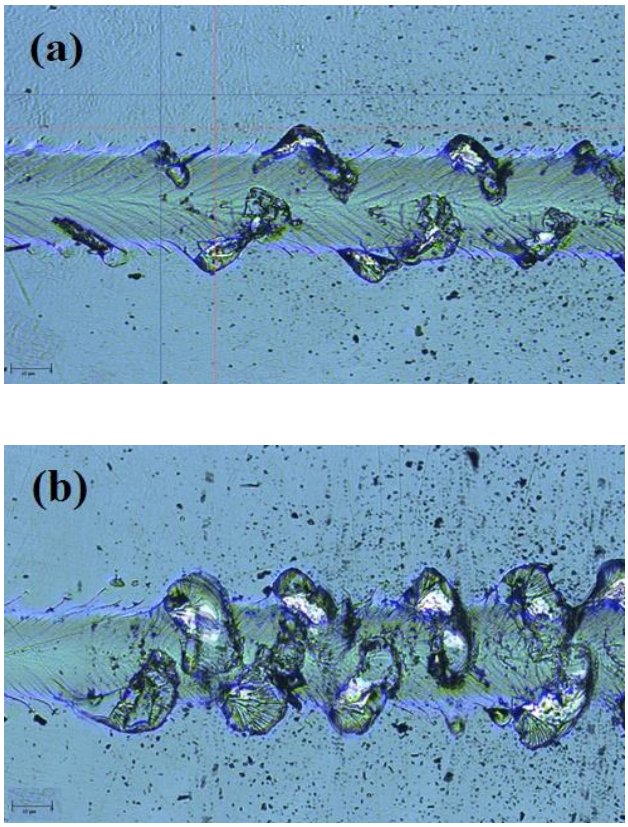

Fig. 7.Surface morphology, along the linear worn track, at region of first delamination which corresponds to L_{c2} vertical load for (a) a-C:H coating and (b) a-C:H:Si coating.

4. Conclusions

a-C:H and a-C:H:Si tribological coatings have been deposited on DIN-100Cr6 bearing steel samples, using an industrial PVD/PACVD equipment. The corrosion resistance have been investigated for these kinds of samples in correlation with hardness, elastic modulus and adherence. The best corrosion behaviour was observed for the a-C:H:Si sample. The presence of Si generally improves the corrosion resistance of the samples.

The highest content of sp^3 bonds is obtained for a-C:H sample. Raman analysis showed that a-C:H:Si film has more sp^2 clustering but the surface becomes smoother, and defects vanish with increasing Si content.

The experimental results revealed lower values of mechanical parameters (hardness, elastic modulus and adherence) in the case of coatings containing Si.

References

[1] Y. Lifshitz, Diamond and Related Materials **8,** 1659 (1999).
[2] J. Robertson, Materials Science and Engineering **37**, 129 (2002).
[3] C. Donnet, Surface and Coatings Technology **180,** 100 (1998).
[4] S.R.P. Silva, J.D. Carey, R.U.A. Khan, E.G. Gerstner, J.V. Anguita, in: H.S. Nalwa (Ed.), Handbook of Thin Film Materials, vol. 4, Academic Press, Ch. **9**, 404 (2002).
[5] C. Corbella, I. Bialuch, M. Kleinschmidt, K. Bewilogua, Solid State Science. **11,** 1768 (2009).
[6] D.F. Franceschini, in: H.S. Nalwa (Ed.), Handbook of Thin Film Materials, vol. 4, Academic Press, 2, Ch. **12,** 649 (2002).
[7] A. Varma, V. Palshin, E.I. Meletis, Surface and Coatings Technology **148,** 305 (2001).
[8] O.K. Porada, V.I. Ivaschenko, L.A. Ivaschenko, G.V. Rusakov, S.N. Dub, A.I. Stegnij, Surface and Coatings Technology **180–181,** 122 (2004).
[9] R. Gilmore, R. Hauert, Thin Solid Films **398–399**, 199 (2001).
[10] M. Grischke, A. Hieke, F. Morgenweck, H. Dimigen, Diamond and Related Materials **7**, 454 (1998).
[11] L.-Y. Chen, F.C.-N.Hong, Diamond and Related Materials **12**, 968 (2003).
[12] J.C. Damasceno, S.S. Camargo, M. Cremona, Thin Solid Films **420–421**, 195 (2002).
[13] M. Ban, T. Hasegawa, Surface and Coatings Technology **162**, 1 (2002).
[14] L. Zajicková, V. Bursiková, V. Perina, A. Macková, J. Janca, Surface and Coatings Technology **174–175**, 281 (2003).
[15] I. Bertóti , A. Tóth, M. Mohai, J. Szépvölgyi, Surface and Coatings Technology**206**, 630 (2011).
[16] Q. Weia, A.K. Sharmaa, J. Sankara, J. Narayana, Composites Part B **30**, 675 (1999).
[17] P. Papakonstantinou, J.F. Zhao, P. Lemoine, E.T. McAdams, J. A. McLaughlin, Diamond and Related Materials **11**, 1074 (2002).
[18] H.G. Kim, S.H. Ahn, J.G. Kim, S.J. Park, K.R. Lee, Diamond and Related Materials **14**, 35 (2005).
[19] C. Bogatu, I. Manciulea, A. Duta, Adv. Mat. Res., **79-82**, 1963 (2009).

[20] I. L. Velicu, M. Neagu, L. Costinescu, D. Munteanu, E. P. Koumoulos, C. A. Charitidis, SensorLetters **11**, 1 (2013).
[21] B. Bhushan, X. Li, Int. Mater.Rev. **48**, 125 (2003).
[22] W. C. Oliver, G. M. Pharr, Journal of Material Research **19**, 3 (2004).
[23] S. Chen, L. Liu, and T. Wang, Surface and Coatings Technology .**191**, 25 (2005).
[24] C. Shaohua, L. Lei, W. Tzuchiang, Acta Mechanica Sinica **20**, 383 (2004).
[25] R. Saha, W. D. Nix, ActaMaterialia **50**, 23 (2002).
[26] H. A. Shivaee, F. Celegato, P. Tiberto, A. Castellero, H. R. M. Hosseini, M. Baricco, Proceedings of the 4th International Conference on Nanostructures (ICNS4), I.R. Iran, March (2012).
[27] D. Munteanu, C. Gabor, D.G. Constantin, B. Varga, R. Adochite, O.C. Andrei, J.M. Chappe,L. Cunha, C. Moura, F. Vaz, Tribology International **44**, 820 (2011).
[28] M-G. Kim, K-R.Lee, K.Y. Eun, Surface and Coatings Technology **112**,204 (1999).
[29] A.C. Ferrari, J. Robertson, Physical Revue B **64**, 075414 (2001).
[30] V. S. Yadav, D. K. Sahu, M. Singh, K. Kumar, Proceedings of the World Congress on Engineering and Computer Science, **I**, 78 (2009).
[31] C. Chen, T. Hong , S. Chen, J. Appl. Phys. **74**, 4483 (1993).
[32] M. Voinea, C. Vladuta , C. Bogatu, A. Duta, Materials Scienceand Engineering B **152,** 76 (2008).
[33] S. Xu, B.K. Tay, H.S. Tan, L. Zhong, Y.Q. Tu, S.P.R. Silva, W.I. Milne, J. Apply. Phys. **79,** 7239 (1996).

* Corresponding author: muntean.d@unitbv.ro